

THE REACTION-DIFFUSION THEORY  
OF MORPHOGENESIS

BY  
CIERRA TINSON

HONORS THESIS

Submitted in partial fulfillment of the requirements  
for the Honors Bachelor of Science in Mathematics  
in the School of Arts and Sciences of the  
University of Rochester, 2022

Rochester, New York

Advisor:

Professor Alex Iosevich

Honors Thesis Committee:

Professor Alex Iosevich

Professor Jonathan Pakianathan

Professor Dan-Andrei Geba

## ABSTRACT

Morphogenesis is the biological process during embryonic development which gives rise to a spectrum of spatially differentiated forms. Since his seminal paper “The Chemical Basis of Morphogenesis” in 1952, Alan Turing’s reaction-diffusion theory for morphogenesis has become a foundational model for studying self-organization behavior and pattern formation in biological, chemical, and physical systems. From how the leopard gets its spots to how panic and disease spreads throughout the masses, seemingly chaotic patterns in nature can be effectively studied with reaction-diffusion theory. While the cellular mechanisms that drive pattern formation and give rise to complex hierarchical structural architectures in natural materials such as bamboo are of great abstract and applied interest, relevant computational models remain largely unexplored. This paper provides (1) an introduction to reaction-diffusion theory and agent-based modeling, (2) a review of biological pattern formation and the role of reaction-diffusion systems for morphogenesis, and (3) an implementation of two cellular models, a cellular automaton (CA) and the cellular Potts model, to simulate Turing patterns under varying inhibitor field values and cell-cell adhesion energy coefficients respectively.

## TABLE OF CONTENTS

I.	INTRODUCTION.....	1
A.	REACTION-DIFFUSION THEORY.....	1
B.	CELLULAR AUTOMATA.....	2
C.	EQUATION-BASED MODELING VERSUS AGENT-BASED MODELING.....	3
II.	BIOLOGICAL PATTERN FORMATION.....	4
A.	ALAN TURING'S REACTION-DIFFUSION MODEL.....	4
B.	NATURAL "TURING" PATTERNS.....	5
C.	EXAMPLE REACTION-DIFFUSION MODELS.....	6
1.	THE FITZ-HUGH NAGUMO MODEL (1961) .....	6
2.	THE GIERER-MEINHARDT MODEL (1972) .....	6
3.	THE SCHNAKENBERG MODEL (1979) .....	6
4.	THE GRAY-SCOTT MODEL (1984) .....	6
III.	MODELING TURING PATTERNS.....	7
A.	DAVID A. YOUNG ACTIVATOR-INHIBITOR MODEL.....	7
1.	THEORETICAL MODEL.....	7
2.	CELLULAR AUTOMATON MODEL.....	8
3.	SIMULATION.....	10
B.	CELLULAR POTTS MODEL (CPM) / GRANER-GLAZIER-HOGEWEG (GGH) MODEL .....	11
1.	THEORETICAL MODEL.....	11
2.	SIMULATION.....	12
IV.	CONCLUDING REMARKS.....	14
	REFERENCES.....	16
	APPENDIX A: CELLULAR AUTOMATA CODE FOR TURING PATTERNS WITH MOORE NEIGHBORHOODS .....	18

<b>APPENDIX B: EXTENDED CELLULAR AUTOMATA.....</b>	<b>22</b>
<b>B1. EVOLUTION OVER TIME (<math>w_2 = 0.2</math>).....</b>	<b>22</b>
<b>B2. VARYING INHIBITOR FIELD VALUE (TIME-STEPS = 20) .....</b>	<b>23</b>
<b>APPENDIX C: COMPUCELL3D CELLULAR POTTS MODEL CODE.....</b>	<b>24</b>
<b>C1. MAIN PYTHON SCRIPT.....</b>	<b>24</b>
<b>C2. XML SCRIPT.....</b>	<b>24</b>
<b>C3. PYTHON SCRIPT.....</b>	<b>25</b>
<b>APPENDIX D: EXTENDED CELLULAR POTTS MODEL RESULTS.....</b>	<b>26</b>

# I. INTRODUCTION

Despite their apparent randomness, patterns are ubiquitous in nature, adhering to predictable structures and orders. Most patterns form naturally from a homogeneous, uniform state, primarily due to self-organizational processes. In self-organizing systems – both physical and biological – local interactions give rise to global spatial and temporal structures. Commonly studied examples include multi-scale hierarchical structures in natural materials (e.g., wood, bone, and bamboo), pedestrian dynamics (e.g., epidemic spread, traffic jams, and crowding), and geological patterning (e.g., drainage patterns, wind ripples in sand, and self-organized vegetation). Understanding the dynamics of cell behavior and pattern formation is of foremost importance in a number of fields, including but not limited to developmental biology, regenerative medicine, and mechanical engineering. Various models have been postulated to explain the formation of these self-organized patterns during the developmental process, the majority classified as a type of “reaction-diffusion” system. The purpose of this paper is to explore the mathematical basis of morphogenesis (the biological process by which cells develop their shape) and some dynamic modeling techniques for simulating individual and collective cell behavior, cell self-organization, and pattern formation.

## A. REACTION-DIFFUSION THEORY

Reaction-diffusion systems are a type of continuous field model in which the state of a system is solely determined by reaction and diffusion processes. In such systems, the concentration of one or more substances in a given space is a result of local reactions between the substances and diffusion of the individual substances throughout the space. Mathematically, reaction-diffusion systems are modeled by non-linear partial differential equations. Reaction-diffusion partial differential equations have the following general form:

$$\frac{\partial f}{\partial t} = R(f) + D\nabla^2 f$$

where  $f(\mathbf{x}, t)$  is a state variable of the system, describing the density of a constituent of the system at position  $\mathbf{x} \in \Omega \subset \mathbb{R}^d$  at time  $t$  ( $\Omega$  a bounded domain),  $R(f)$  describes the reaction kinetics of the system,  $D$  is the diffusion coefficient, and  $\nabla^2$  denotes the Laplace operator.

If there are  $n$  coupled reactions involving constituents  $f_i$ , then the array of reaction diffusion equations is

$$\begin{aligned}\frac{\partial f_1}{\partial t} &= R_1(f_1, f_2, \dots, f_n) + D_1 \nabla^2 f_1 \\ \frac{\partial f_2}{\partial t} &= R_2(f_1, f_2, \dots, f_n) + D_2 \nabla^2 f_2 \\ &\vdots \\ \frac{\partial f_n}{\partial t} &= R_n(f_1, f_2, \dots, f_n) + D_n \nabla^2 f_n\end{aligned}$$

where  $R_i(f_1, \dots, f_n)$  describes the local dynamics of constituents (independent of spatial derivatives) and  $D_i \nabla^2 f_i$  are the diffusion terms [15].

## B. CELLULAR AUTOMATA (Ishida, micromachines, 2018)

A cellular automaton is a discrete, rule-based computational model. Invented by John von Neumann and Stanislaw Ulam in the 1950s for understanding machine self-replication, cellular automata have since been developed for other applications, including but not limited to (1) modeling the dynamic behavior of individual and collective biological cells, (2) high-speed computing and information processing, and (3) simulating phenomena in fields such as physics and chemistry, as well as phenomena observed in physical systems. It has been theorized that cellular automata introduce the possibility of controlling self-organized patterns such as those observed in tissue, bone, and other natural materials.

A cellular automaton is an  $n$ -dimensional array of cells ( $n = 1, 2, 3$ ) which evolve in [discrete] space and time according to a defined set of stepwise transition rules and local interactions in a defined neighborhood (namely, the set of nearby cells with which a cell-of-interest can interact). Two common types of neighborhoods include von Neumann's diamond-shaped regions and Moore's square-shaped regions (see Fig. 1).

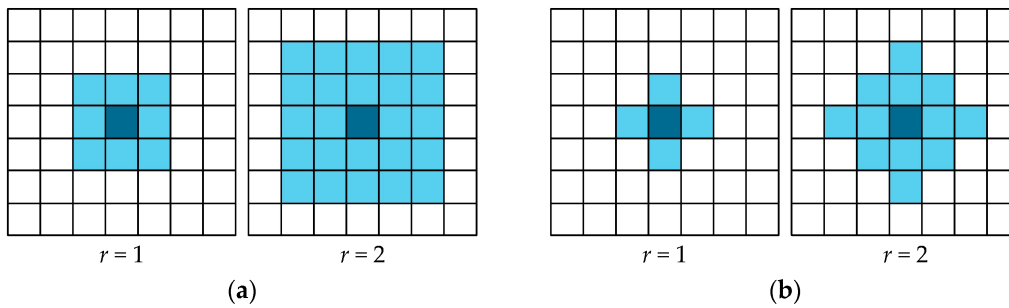


FIG. 1. The symmetry of (a) Moore neighborhoods and (b) von Neumann neighborhoods for a two-dimensional cellular automaton. [3]

### C. EQUATION-BASED MODELING VERSUS AGENT-BASED MODELING

Two main approaches are used to model the spatiotemporal behavior of a system: agent-based modeling and equation-based modeling. Agent-based modeling is a bottom-up approach: the individuals of a system are initially regarded as autonomous agents with different properties and behaviors, and the outcome of the system emerges as a result of agent interactions. Conversely, equation-based modeling is more reminiscent of a top-down approach: the overall behavior of the system is modeled using a set of equations representing system variability over time (ordinary differential equation) or over time and space (partial differential equations). Agent-based models are advantageous as a discrete model for systems characterized by high degrees of localization and distribution, whereas equation-based models are preferable when representing the overall behavior and physical processes of a system. [18]

Various equation-based models exist, the most notable being ordinary differential equations and partial differential equations. Similarly, there are two main categories of agent-based models: on lattice models (discrete time and space) and off lattice models (continuum of time and space). For modeling multicellular systems, the prominent on lattice models include cellular automata and the cellular Potts model, and the prominent off lattice models include center-based models and deformable cell models (see Fig. 2).

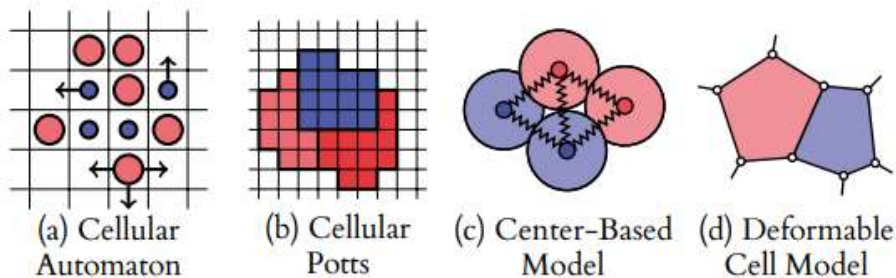


FIG. 2. The four main categories of agent-based models. [2]

Although they are classified differently, cellular Potts models are in actuality a type of cellular automaton used to describe biophysical systems and cell populations. In the Potts model, individual and collective cell behavior is dictated by pre-described energy kinetics using a built-in Hamiltonian (an operator corresponding to the total energy of the system). While on-lattice models consider a physical system prescribed to a set of lattice points (e.g., a real coordinate space), off-lattice models consider agents which diffuse continuously through space. In center-based models, cells are identified as points moving in continuous space, able to interact with their neighbors through adhesion and repulsion forces. Similarly, in deformable cell models, the shape of each cell is modeled explicitly and changes according to the pressure forces from neighboring cells. [2]

## II. BIOLOGICAL PATTERN FORMATION

Morphogenesis is the biological process through which an initially uniform field of cells acquires complex, organized, and spatially differentiated forms. British mathematician Alan Turing was among the first to propose a theoretical mechanism for how various self-organized patterns form autonomously in an organism. In his 1952 paper “The Chemical Basis of Morphogenesis,” Turing postulated that identical biological cells differentiate due to intercellular reaction-diffusion processes. More specifically, despite the possible initial homogeneity of a chemical system, patterns and structures may form “due to an instability of the homogeneous equilibrium, which is triggered off by random disturbances” [1].

### A. ALAN TURING’S REACTION-DIFFUSION MODEL

Consider two chemical substances, called morphogens, homogeneously distributed throughout a medium of fixed space. The two morphogens (say  $U$  and  $V$ ) undergo local chemical reactions with each other and which diffuse throughout the medium at different rates. In the absence of diffusion, the morphogens remain in the stable, homogeneous state. By introducing spatial dependence and diffusion processes, the homogeneous state is destabilized, and a non-homogeneous state arises. During this destabilization, morphogenic interactions establish chemical gradients and autonomously generate various spatial patterns. A general form of Turing’s reaction-diffusion partial differential equation model for two chemical substances is as follows:

$$\begin{aligned}\frac{\partial U}{\partial t} &= f(U, V) + D_U \nabla^2 U \\ \frac{\partial V}{\partial t} &= g(U, V) + D_V \nabla^2 V\end{aligned}$$

where  $U$  and  $V$  are the morphogen concentrations,  $f(U, V)$  and  $g(U, V)$  are the [local] reaction kinetics (describing the production and decay of morphogens),  $D_U$  and  $D_V$  are the morphogen diffusion coefficients, and  $\nabla^2$  is the Laplace operator.

From this model, Turing predicted six stable-state solutions, independent of the initial conditions of the system: uniform (I) stationary and (II) oscillatory states, [extremely] short wavelength (III) stationary and (IV) oscillatory states, and finite wavelength (V) oscillatory and (VI) stationary states. The sixth stable solution predicted by Turing’s model – stationary waves with finite wavelength – are of particular interest in physical and biological pattern formation.

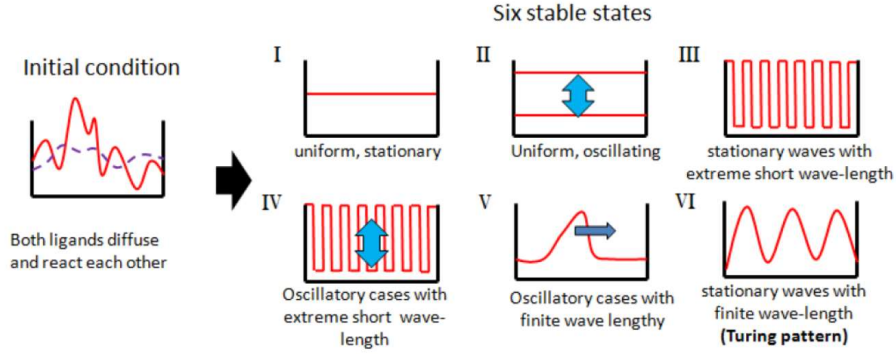


FIG. 2. Six potential steady states predicted by Turing’s model, independent of the initial condition. [7]

## B. NATURAL “TURING” PATTERNS

Under certain conditions, various non-homogeneous patterns (e.g., patches, spots, stripes, and rosettes) emerge from this solution, their spatial heterogeneity reminiscent of naturally occurring patterns in nature – the so called “Turing Patterns.” Said patterns emerge from the “stationary waves with finite wave-length” stable solution, as indicated by Fig. 2 above. Though Turing patterns are most often associated with morphogenesis and animal pigmentation patterns (see Fig. 3), they are also observable in larger-scale physical systems.

Turing patterns emerge from a series of small perturbations in the homogenous concentrations, becoming stable over time. The first morphogen (say  $U$ ) is an activator, capable of inducing activator concentrations in local cells through short-range interactions. The second morphogen (say  $V$ ) is an inhibitor, restraining activator growth in nearby cells. Although the exact values differ, the diffusivity  $U$  is typically much less than the diffusivity of  $V$  during morphogenesis; the combination of a slowly diffusing activator and a quickly diffusing inhibitor resulting in coupled short-range activation and long-range inhibition. Cell activity is driven by morphogenic concentrations from nearby cells, transforming via local chemical reactions and spreading out through the medium.



FIG. 3. Reaction-diffusion simulations and corresponding color patterns in nature. [8]

## C. EXAMPLE REACTION-DIFFUSION MODELS

Since Turing's seminal 1952 paper (published only a year after he first turned his attention to biomathematics), many coupled systems of reaction-diffusion equations have emerged to model autonomous pattern formation in biological systems. For the sake of brevity, four widely studied systems are summarized below, though other notable models include the Thomas-Murray Model and the Brusselator Model. In the following models,  $U$  and  $V$  are the concentrations of two generic chemical species  $u$  and  $v$  with respective diffusivity terms  $D_U \nabla^2 U$  and  $D_V \nabla^2 V$ . The remaining terms describe the reaction kinetics of the system for fixed constants  $a, \epsilon, \rho, \mu$ , etc. The complete models given below can be found in references [4], [6], [16], and [9] respectively.

### 1. THE FITZ-HUGH NAGUMO MODEL (1961)

$$\begin{aligned}\frac{\partial U}{\partial t} &= (a - U)(U - 1)U - V + D_U \nabla^2 U \\ \frac{\partial V}{\partial t} &= \epsilon(bU - V) + D_V \nabla^2 V\end{aligned}$$

### 2. THE GIERER-MEINHARDT MODEL (1972)

$$\begin{aligned}\frac{\partial U}{\partial t} &= \rho \left( \frac{U^2}{h} - \mu U \right) + D_U \nabla^2 U \\ \frac{\partial V}{\partial t} &= \rho(V^2 - \nu h) + D_V \nabla^2 V\end{aligned}$$

### 3. THE SCHNAKENBERG MODEL (1979)

$$\begin{aligned}\frac{\partial U}{\partial t} &= a - U + U^2 V + D_U \nabla^2 U \\ \frac{\partial V}{\partial t} &= b - U^2 V + D_V \nabla^2 V\end{aligned}$$

### 4. THE GRAY-SCOTT MODEL (1984)

$$\begin{aligned}\frac{\partial U}{\partial t} &= D_U \nabla^2 U - UV^2 + F(1 - U) \\ \frac{\partial V}{\partial t} &= D_V \nabla^2 V + UV^2 - (F + k)V\end{aligned}$$

### III. MODELING TURING PATTERNS

Two computational approaches have been used successfully to model pattern formation. The first is a cellular automata model, a rule-based alternative to Turing’s reaction-diffusion partial differential equation system. The second is a cellular Potts model, a cellular and tissue-formation computational system used to simulate individual and collective cell behavior and tissue morphogenesis. Natural [Turing] patterns are initially derived from the cellular automata solution for the generalized reaction-diffused system and are then replicated in cellular Potts models by altering cellular parameters such as cell-cell adhesion energy coefficients.

#### A. DAVID A. YOUNG ACTIVATOR-INHIBITOR MODEL [21]

In his 1984 paper “A Local Activator-Inhibitor Model of Vertebrate Skin Patterns,” David Young proposed an activator-inhibitor diffusion theory as an alternative to the Turing model for skin pigmentation patterns (an extension of N.V. Swindale’s 1980 model for pattern formation in the visual cortex of the brain). Contrary to the Turing model, Young theorized that “the intercellular interaction [of pigment cells] is local, possibly due to short-range diffusion of morphogen molecules or to direct cell contact,” and the initial and boundary conditions as well as the various cell interactions give rise to a spectrum of pigment patterns.

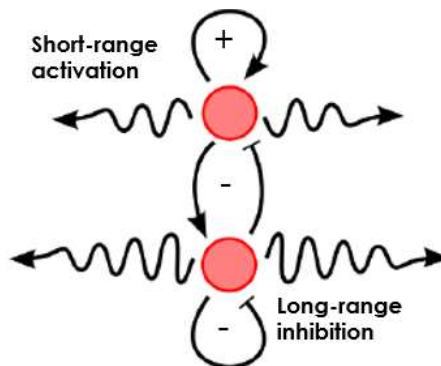


FIG. 4. The canonical two-component “activator-inhibitor” Turing system, as proposed by Young. [10]

#### 1. THEORETICAL MODEL

Young’s model starts by assuming a uniform distribution of two types of pigments cells – differentiated (colored) cells (DCs) and undifferentiated cells (UCs) – on the early embryonic skin of a vertebrate. Each DC produces two morphogens at a constant rate, an activator  $M^{(1)}$  and an inhibitor  $M^{(2)}$ , while the UCs are passive and produce no active

substances. Both the inhibitor morphogens and the activator morphogens are diffusible substances, uniformly degraded by the surrounding cells. The inhibitor morphogens simulate the dedifferentiation of nearby DCs while the activator morphogens stimulate the differentiation of nearby UCs.

The production, diffusion, and decay processes for a morphogen can mathematically be represented by the generalized diffusion equation,

$$\frac{\partial M}{\partial t} = \nabla \cdot \mathbf{D} \cdot \nabla M - KM + Q$$

where  $M = M(\mathbf{r}, t)$  is the activator (or inhibitor) morphogen concentration,  $\nabla \cdot \mathbf{D} \cdot \nabla M$  is the diffusion process of  $M$ ,  $KM$  is the first-order chemical transformation of  $M$ , and  $Q$  is the production rate of  $M$ . The results of these substance interactions are dependent on four variables per morphogen: (1) the rate of production, (2) the rate of degradation, (3) the rate of diffusion, and (4) the strength of their activating/inhibiting interactions.

Conventionally, the activator morphogens  $M^{(1)}$  are diffusing at a much slower rate than the inhibitor morphogens  $M^{(2)}$ , inducing short-range activation regions and long-range inhibition regions, respectively. For each morphogenic pair produced by a DC, the steady-state distributions of their concentrations constitute a morphogenic field  $w(R)$  of radius  $R$ , centered at the DC. The state of each pigment cell (DC and UC) is driven by the net activation-inhibition effect of the neighboring DCs. A net activation effect is denoted by a positive field value, and the net inhibition effect is denoted by a negative field value.

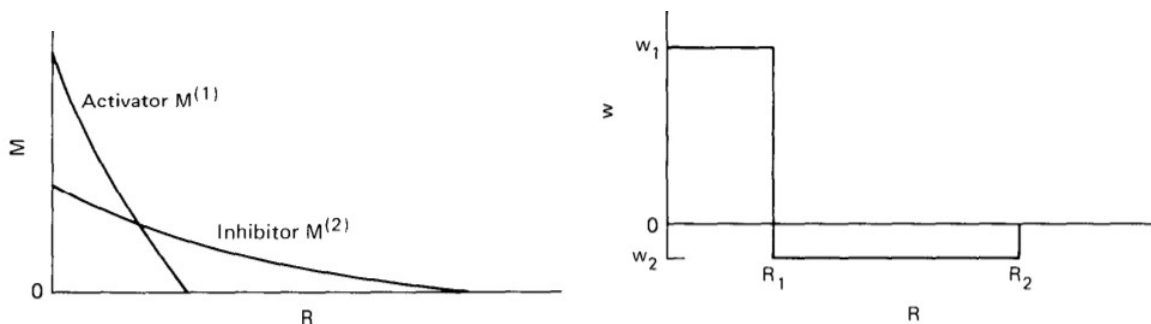


FIG. 5. A schematic illustration of the local activator-inhibitor model as provided by Young, showing (left) the steady-state activator and inhibitor concentrations against their ranges and (right) the net effect of the activator-inhibitor field, where  $w(R)$  is the morphogenic field read at distance  $R$  from a DC. [21]

## 2. CELLULAR AUTOMATON MODEL

In the next section of his paper, Young describes how to convert his local activator-inhibitor continuum model for pattern formation into a cellular automaton. To do so, Young discretizes cell positions on a rectangular grid of points – each point representing

one DC or UC pigment cell – and assumes an initial random distribution of the DCs throughout the grid. He then simplifies the morphogenic field as follows:

For each grid point at position  $\mathbf{R}$ , the field values due to all nearby DCs at positions  $\mathbf{R}_i$  are added up. If  $\sum_i w(|\mathbf{R} - \mathbf{R}_i|) > 0$ , then the point at  $\mathbf{R}$  becomes (or remains) a DC. If  $\sum_i w(|\mathbf{R} - \mathbf{R}_i|) = 0$ , then the point does not change state, and if  $\sum_i w(|\mathbf{R} - \mathbf{R}_i|) < 0$ , the point becomes (or remains) a UC.

Assuming the activation area has a radius of 2.30, the inhibition area has a radius of 6.01, and the activation field value  $w_1$  is +1.0, Young produced the following patterns by varying the inhibition field value  $w_2$  as indicated at the bottom of each image:

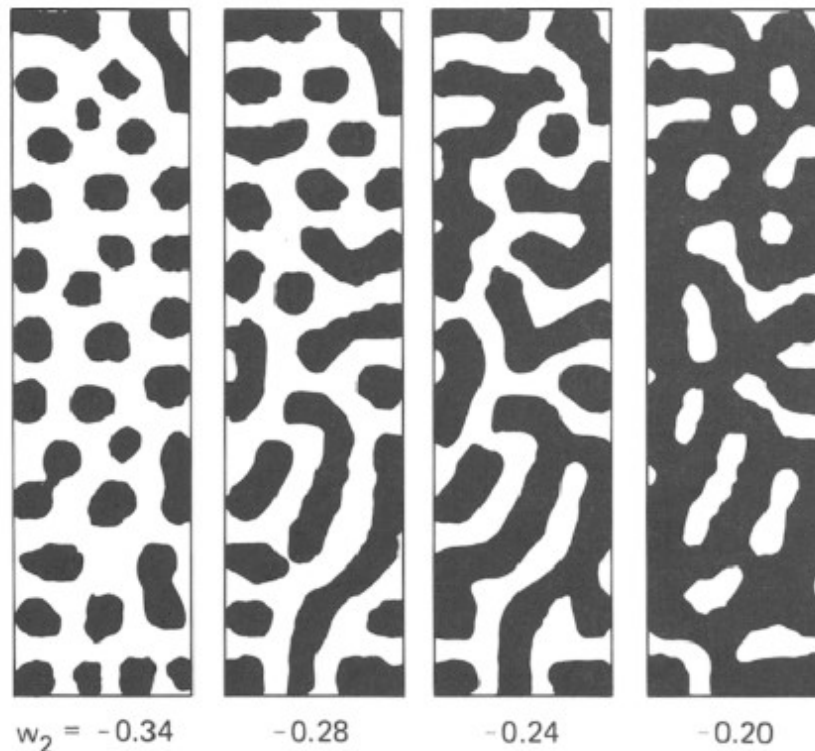


FIG. 6. Turing-like patterns produced by Young using his activator-inhibitor model. [21]

Young noted that the general form of the final [stable] pattern is independent of the initial distribution of the DCs. Moreover, when the inhibitor field value is high (relative to the activator field value), the DCs are restrained in a way so as to only be able to form isolated spots. As the inhibitor field value decreases and the activator field value dominates, the DCs self-organize into spots and connect up to stripes.

### 3. SIMULATION

Young's cellular automata model was replicated in Python using a similar prescribed set of transition rules, a 2-dimensional grid, and Moore neighborhoods. As in Young's model, four model parameters were considered:

- $r_1$ : Radius of activation
- $r_2$ : Radius of inhibition
- $w_1$ : Weight of activation (normalized to +1)
- $w_2$ : Weight of inhibition

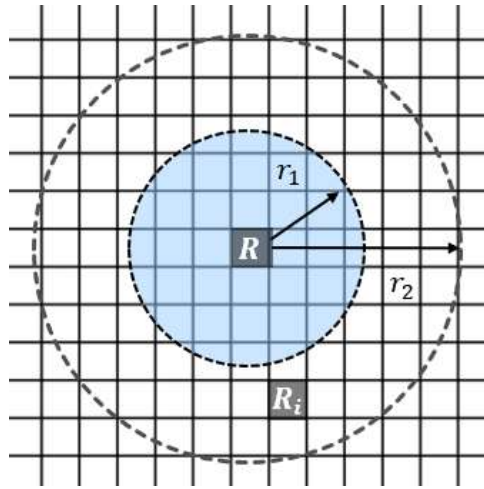


FIG. 7. Outline of Young's model. The focal cell is located at  $R$  and the neighboring cell at  $R_i$ .

For the following simulations, the probability that a cell is initially a differentiated (DC) or colored (UC) cell was also parameterized. The cell-state transition rules are as follows:

*Short-Range Activation:*

$$\text{Cell State} = 1 \text{ if } \sum_i w_2(|R - R_i|) > 0$$

*Long-Range Inhibition:*

$$\text{Cell State} = 0 \text{ if } \sum_i w_2(|R - R_i|) < 0$$

*Stable State:*

$$\text{Cell State} = \text{Unchanged if } \sum_i w_2(|R - R_i|) = 0$$

To check the validity of the model, simulations were run using the same parameters as Young: the radius of activation was  $r_1 = 2.30$ , the radius of inhibition was  $r_2 = 6.01$ , and the weight of activation was  $w_1 = 1.00$ . Periodic boundary conditions and Moore neighborhoods were assumed. The probability a cell was initially a differentiated cell was  $p = 0.015$  and the weight of inhibition  $w_2 < 0$  was varied. Each simulation is run for 30 time-steps to yield the following stable patterns:

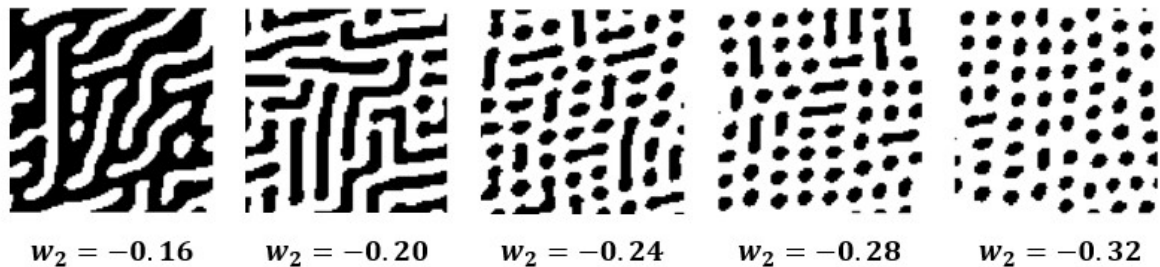


FIG. 8. Patterns produced using the activator-inhibitor cellular automaton simulations written in Python.

As expected, the patterns produced by the cellular automaton devolved from stripes to spots as the inhibition field value  $w_2$  was increased (Fig. 8, left to right). Extended results are given in Appendix B.

## B. CELLULAR POTTS MODEL (CPM) / GRANER-GLAZIER-HOGEWEG (GGH) MODEL

A cellular Potts model (CPM), also known as the Glazier-Graner-Hogeweg (GGH) model, is a spatial lattice-based computational modeling method for cells and tissue. Originally proposed by François Graner and James Glazier in 1992 for the simulation of biological cell sorting, CPMs gained popularity for studying morphogenesis in 1997 by Paulien Hogeweg. They have since been extensively used for modeling the complex dynamics and spatiotemporal behavior of biological cell populations, including tumor growth.

### 1. THEORETICAL MODEL

The cellular Potts model is characterized by a set of generalized cells on a lattice, internal states for each cell, and auxiliary fields such as diffusing chemicals. In the original Graner-Glazier model, cells of two types were assumed, with different adhesion energies for cells of the same type and cells of a different type. Both types of cells were also assumed to have a different contact energy with the medium and cell volume was assumed to remain close to a target volume. An example of a cellular Potts model and the corresponding lattice for two cell types is given in Fig. 9. The dynamics of the cellular Potts model are

governed by the Hamiltonian, which describes the total energy of the multicellular system in a given configuration on the lattice. The individual and collective cells generally act in such a way that minimizes the value of the Hamiltonian  $H$  of the system,

$$H = \sum_{i, j \text{ neighbors}} J(\tau(\sigma_i), \tau(\sigma_j)) (1 - \delta(\sigma_i, \sigma_j)) + \lambda \sum_{\sigma_i} (v(\sigma_i) - V(\sigma_i))^2$$

$\sigma_i \equiv$  Cell at site  $i$

$\tau(\sigma_i) \equiv$  Cell type of cell  $\sigma_i$

$J(\tau(\sigma_i), \tau(\sigma_j)) \equiv$  Adhesion coefficient between two cells of types  $\tau(\sigma_i)$  and  $\tau(\sigma_j)$  respectively

$\delta(\sigma_i, \sigma_j) \equiv$  Kronecker delta

$\lambda \equiv$  Lagrange multiplier for the strength of the volume constraint (the “lambda volume”)

$v(\sigma_i) \equiv$  Volume of cell  $\sigma_i$

$V(\sigma_i) \equiv$  Target volume of cell  $\sigma_i$

for lattice sites  $i$  and  $j$  [7]. Similar to the inhibition field value for the cellular automaton model of morphogenesis, a spectrum of different cell sorting behaviors will expectedly emerge by varying the adhesion coefficients between cells of the same type and of different types.

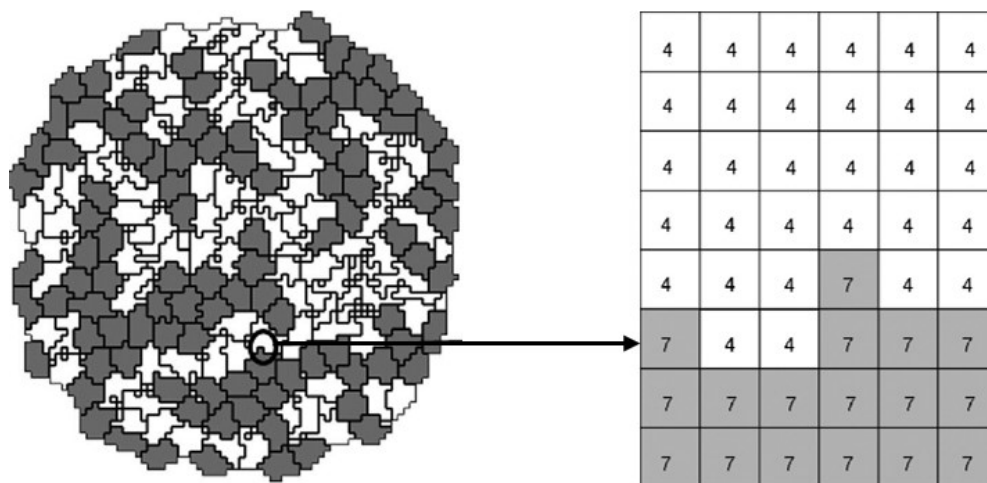


FIG. 9. Detail of a typical 2D Graner-Glazier-Hogeweg (GGH) cell-lattice configuration. Each generalized cell is a set of cell-lattice sites. [17]

## 2. SIMULATION

A CPM was implemented in CompuCell3D (CC3D), a three-dimensional C++ software designed for modeling the dynamics of autonomous multicellular biological systems. By varying the biological properties and energy rules of cells, a spectrum a cellular behavior such as morphogenesis emerges. In an attempt to derive the cellular mechanisms that

drive the formation of Turing patterns, two cell types – condensing “Type 1” cells (blue) and non-condensing “Type 2” cells (green) – as well as the surrounding medium (black) were considered. Simulation parameters were defined as follows:

$$\begin{aligned}
 v_{target} &= 25 \mu m^3 \\
 v_{\lambda} &= 2 \mu m^3 \\
 J_{M-1} &= J_{M-2} = J_{1-2} = 16 \frac{J}{\mu m^3} \\
 J_{1-1} \ \& \ J_{2-2} &\in \{0.5, 1, \dots, 17.5, 18\} \frac{J}{\mu m^3}
 \end{aligned}$$

where  $J_{p-q}$  refers to the adhesion energy coefficient for interacting cells of type  $p$  and  $q$ . Each simulation was run for approximately 3000 Monte Carlo Steps, or until the patterns stabilized in time (the number of steps given by the CC3D program).

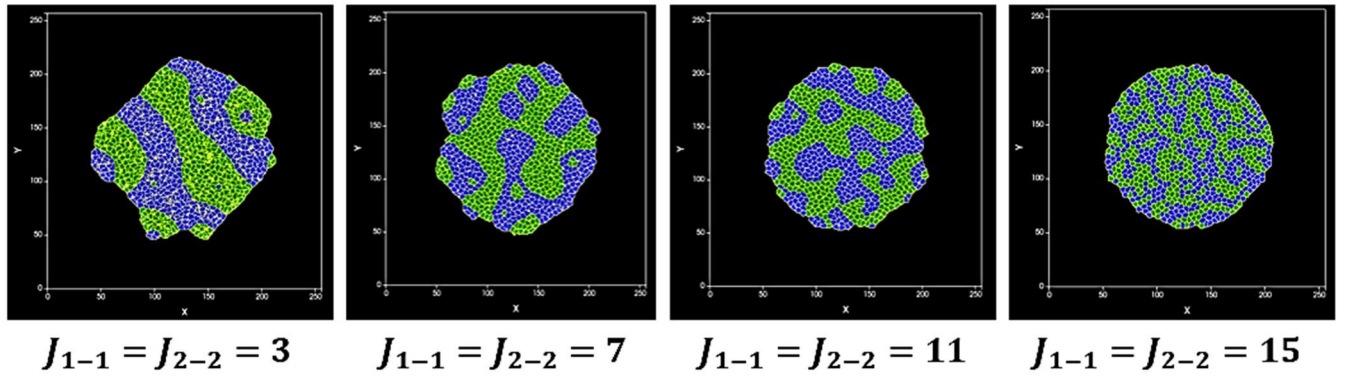


FIG. 10. Patterns produced using the CompuCell3D cellular Potts model.

Some of the results generated are given above in Fig. 10 and extended results are provided in Appendix D. When the adhesion energy between cells of the same type was small in comparison to the adhesion energy between cells of distinct types, the condensing cells grouped to form thick and distinct stripes. As the adhesion energy between cells of the same type increased, the stable patterns produced by the CPM became a combination of stripes and spots before forming a maze-like pattern. If the adhesion energy between cells of the same type was greater than the adhesion energy between cells of distinct types, then the individual condensing cells became evenly distributed among the non-condensing cells.

#### IV. CONCLUDING REMARKS

Certain natural materials (e.g., trabecular [spongy] bone, tissue, cuticle, culm, bamboo, nacre, and wood) exhibit multi-scale hierarchical structures. These complex structural architectures arise as a result of self-organization processes at different length scales in the material during development. Consequently, these materials have superior mechanical properties compared to synthetic materials like plastics and metals. For example, these natural materials have a higher specific yield strength while requiring less energy to be produced. The specific strength of bamboo ( $\sim 114 \text{ MPa} \times \text{cm}^3/\text{g}$ ) is 3-4 times greater than that of structural steel ( $\sim 32 \text{ MPa} \times \text{cm}^3/\text{g}$ ), and the energy required to produce bamboo (below  $1 \text{ MJ}/\text{kg}$ ) is significantly less than that of steel ( $25 \text{ MJ}/\text{kg}$ ). The cellular mechanisms that form such architectural patterns are of great interest in the design of lightweight engineering structures as well as in the design and fabrication of tissues and organs using 3D bioprinting methods.

Understanding what drives these patterns to form may function as a guide for the synthesis of material microstructures, though relevant computation models remain unexplored. As discussed, and demonstrated, in this paper, cell sorting behavior, pattern formation and morphogenesis can be studied using discrete dynamical systems such as the cellular automaton and the cellular Potts model. Despite the simplistic nature of both the cellular automaton and cellular Potts model used, each has been successfully used for the replication of natural ‘‘Turing’’ patterns (see Fig. 11).

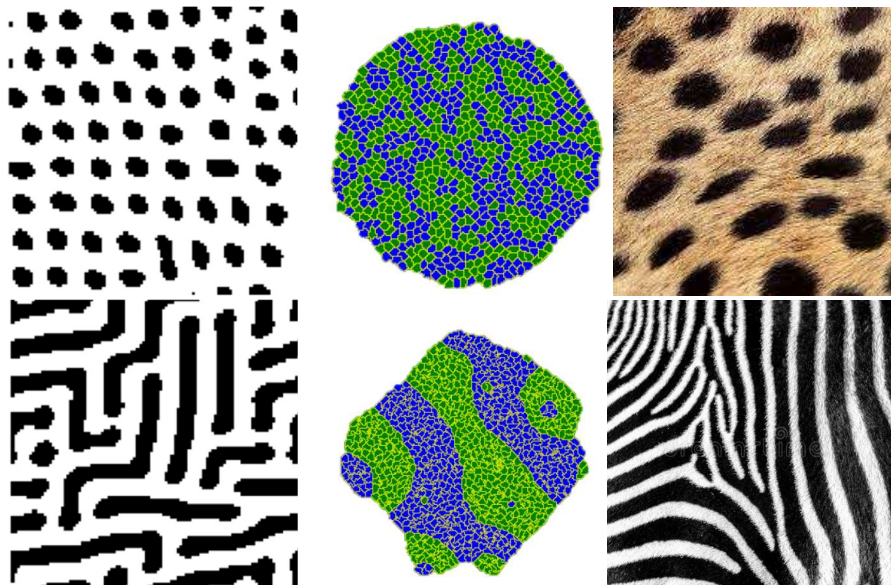


FIG. 11. Patterns formed by the cellular automata, the cellular Potts model, and by nature. Assuming the same simulation parameters are before, an inhibition field value of  $w_2 = -0.20$  and a cell-cell adhesion coefficient of  $J_{1-1} = J_{2-2} = 15$  correspond to leopard spots (top) [14]. Similarly, a combination of  $w_2 = -0.32$  and  $J_{1-1} = J_{2-2} = 3$  correspond to zebra stripes (bottom) [20].

It has been observed that an increasing inhibition field value  $w_2$  roughly correlates to a decreasing adhesion energy coefficient  $J$  between cells of the same type, while also indicating that intercellular adhesion is one of the driving forces for morphogenesis. It was also observed that increasing the inhibition field value (alternatively, decreasing the cell-cell adhesion energy coefficients for cells of the same type) produces patterns that connect down from stripes to spots. To continue to understand the architectural patterns found in natural hierarchical structures – such as that seen in Fig. 12 for bamboo – future models should include a way of approximating the strain-energy field (such as with finite element analysis) and expanding to pattern formation across multiple length scales.

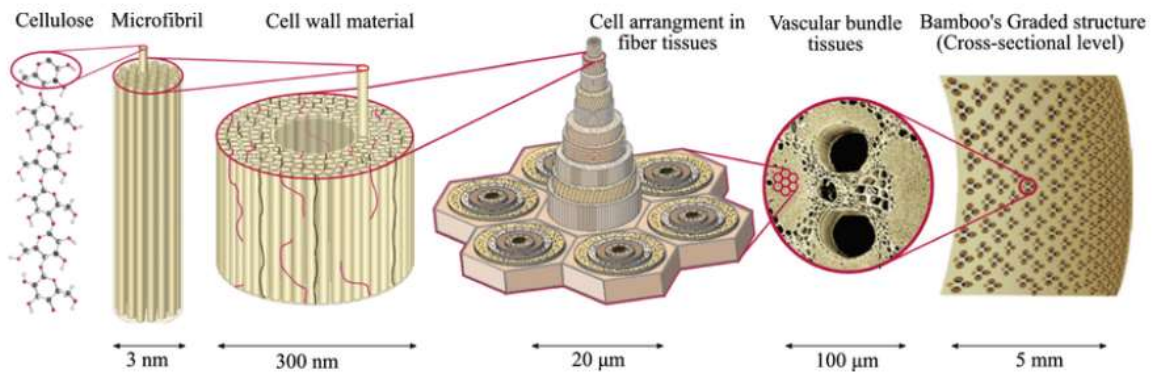


FIG. 12. Hierarchical structure of bamboo. [4]

## REFERENCES

- [1] V. Balbi (2015), *Modeling morphogenesis in living matter*, Solid Mechanics Doctoral Dissertation, Université Pierre et Marie Curie-Paris VI. [2](#)
- [2] A. Coulier (2021), *Multiscale Modeling in Systems Biology, Methods and Perspectives*, Doctoral Dissertation, Acta Universitatis Upsaliensis.
- [3] O. Evsutin, A. Shelupanov, R. Meshcheryakov, D. Bondarenko, and A. Rashchupkina (2016), *The Algorithm of Continuous Optimization Based on the Modified Cellular Automaton*, *Symmetry* **8**(9), p. 84.
- [4] R. Fitzhugh (1961), *Impulses and Physiological States in Theoretical Models of Nerve Membrane*, *Biophysical journal* **1** (6), pp. 445-466.
- [5] T. Gangwar, J. Heuschele, G. Annor, A. Fok, K. Smith, and D. Schillinger (2021), *Multiscale characterization and micromechanical modeling of crop stem materials*, *Biomechanics and Modeling in Mechanobiology* **20** (1), pp. 69-91.
- [6] A. Gierer and H. Meinhardt (1972), *A theory of biological pattern formation*, *Kybernetik* **12** (1), pp. 30-39.
- [7] J. A. Glazier, A. Balter, and N. J. Poplawski (2007), *Magnetization to Morphogenesis: A Brief History of the Glazier-Graner-Hogeweg Model*, *Mathematics and Biosciences in Interaction*, pp. 79-106. [8](#), [10](#)
- [8] F. Graner and J. A. Glazier (1992), *Simulation of biological cell sorting using a two-dimensional extended Potts model*, *Physical review letters* **69** (13), pp. 2013-2016. [7](#)
- [9] P. Gray and S. K. Scott (1984), *Autocatalytic reactions in the isothermal, continuous stirred tank reactor: Oscillations and instabilities in the system  $A + 2B \rightarrow 3B, B \rightarrow C$* , *Chem. Eng. Sci.* **39**, pp. 1087-1097.
- [10] J. Hsia, W. Holtz, D. Huang, M. Arcak, and M. M. Maharbiz, (2011), *A quenched oscillator network for pattern formation in gene expression*, *Proceedings of the American Control Conference*, pp. 2284-2289.
- [11] S. Kondo and T. Miura (2010), *Reaction-Diffusion Model as a Framework for Understanding Biological Pattern Formation*, *Science* **329** (5999), pp. 1616-1620. [9](#)
- [12] H. C. Metz, M. Manceau, and H. E. Hoekstra (2011), *Turing patterns: how the fish got its spots*, *Pigment Cell & Melanoma Research* **24** (1), pp. 12-14. [6](#)
- [13] J. D. Murray (2003), *Mathematical Biology II: Spatial Models and Biomedical Applications*, *Interdisciplinary Applied Mathematics* **18**, Springer, New York.
- [14] [Photograph of leopard spots], <http://www.cheetahkids.com/cheetah-info/more-than-spots/>.
- [15] H. Sayama (2015), *Reaction-Diffusion Systems*, *Introduction to the Modeling and Analysis of Complex Systems* **1**, Open SUNY Textbooks, pp. 259-268. [1](#)
- [16] J. Schnakenberg (1979), *Simple chemical reaction systems with limit cycle behavior*, *Journal of Theoretical Biology* **81** (3), pp. 389-400.

- [17] M. H. Swat, G. L. Thomas, J. M. Belmonte, A. Shirinifard, D. Hmelijak, and J. A. Glazier (2012), *Computational Methods in Cell Biology*, *Methods in Cell Biology* **110**, pp. 325-366.
- [18] System Sciences at SIS (n.d.), *Equation-based versus agent-based modeling*, Institute of System Sciences, Innovation and Sustainability Research SIS, the University of Graz. **3**
- [19] A. M. Turing (1952), *The Chemical Basis of Morphogenesis*, *Philosophical Transactions of Royal Society of London, Series B, Biological Sciences* **237 (641)**, pp. 37-72.
- [20] K. Vartzbed (n.d.), *Real black and white zebra stripes photo pattern of nature design*.
- [21] D. Young (1984), *A Local Activator-Inhibitor Model of Vertebrate Skin Patterns*, *Mathematical Biosciences* **72 (1)**, pp. 51-58. **4**

## APPENDIX A: CELLULAR AUTOMATON CODE FOR TURING PATTERNS WITH MOORE NEIGHBORHOODS

```
#!/usr/bin/env python
# coding: utf-8

# In[1]:

# Import the necessary libraries/packages
import numpy as np
import random
import matplotlib.pyplot as plt
import pylab

# In[2]:

# Cell grid / lattice
width = 100
height = 100

# In[3]:

# There is a probability  $p$  that a cell is initially assigned to be a DC (differentiated, or
colored, cell)
# All other cells are undifferentiated cells (UC's)
p = 0.015

# In[4]:

# Radii of neighborhoods ( $0 < R_a < R_i$ )
Ra = 2 # For activation (inner radii)
Ri = 5 # For inhibition (outer radii)

# In[5]:

# Weight of the neighborhoods (representing their relative strengths)
wa = 1 # Activation field value
wi = 0.2 # Inhibitor field value
```

```

# In[6]:

# Initialize the random number generator
random.seed()

# In[7]:

# Initial state of all cells is 0 (passive)
grid = np.zeros([height, width])

# Initial state of all cells after one timestep is 0
# Note: new_grid is populated with the next states of the cells at the time of state
updating
new_grid = np.zeros([height, width])

time = 0 # Start simulation at 0 seconds

for x in range(width):
    for y in range(height):

        # If the random value assigned to the cell is less than the probability that a cell is
        initially a DC
        if random.random() < p:
            state = 1 # Cell is in an active state

        # If the random value assigned to the cell is greater than or equal to the probability
        of the cell being a UC
        else:
            state = 0 # Cell is in a passive state

        # Update the grid with the states of the cells
        grid[y, x] = state

# In[8]:

```

*# Simulate the evolution of the system*

**def** step(grid, new\_grid):

**for** x **in** range(width):

**for** y **in** range(height):

*# Retrieve current state of the cell: Active or Passive*

state = grid[y, x]

*# Neighborhood of activation*

Na = 0

*# Neighborhood of inhibition*

Ni = 0

*# Consider relative coordinate variables, dx and dy, ranging from -1 to 1*

*# Sweep through the neighbor cells for the state-transition function*

*# Use mod operator to implement periodic boundary conditions*

*# Periodic BC's implies that the patterns will seamlessly tile the plane*

**for** dx **in** range(-Ra, Ra + 1):

**for** dy **in** range(-Ra, Ra + 1):

Na += grid[(y + dy) % height, (x + dx) % width]

**for** dx **in** range(-Ri, Ri + 1):

**for** dy **in** range(-Ri, Ri + 1):

Ni += grid[(y + dy) % height, (x + dx) % width]

*# The state of the cell depends on the sum of the states of the local cells*

*# Calculate the weighted sum of the activating cells and inhibiting cells in the neighborhood*

WS = Na \* wa - Ni \* wi

*# Short-range activation*

*# Weighted sum of activating cells is greater than weighted sum of inhibiting cells*

**if** WS > 0:

state = 1

```

    # Long-range inhibition
    # Weighted sum of activating cells is less than weighted sum of inhibiting cells
    elif WS < 0:
        state = 0

    # Cell does not change state
    # Weighted sum of activating cells equals weighted sum of inhibiting cells
    else:
        state = grid[y, x]

    # Determine the next state of the model
    new_grid[y, x] = state

return new_grid

# In[9]:

# Show the state of the CA at the end of the simulation for fixed time t
fig = plt.figure()

plt.figtext(0.5, -0.25,
            'p = ' + str(p) +
            '\nR{activation}$ = ' + str(Ra) +
            '\nw{activation}$ = ' + str(wa) +
            '\nR{inhibition}$ = ' + str(Ri) +
            '\nw{inhibition}$ = ' + str(wi),
            wrap = True,
            horizontalalignment = 'center',
            fontsize = 12)

# Run the CA for a fixed amount of time
for time in range(21):
    plt.pcolor(grid, vmin = 0, vmax = 1, cmap = "binary")
    plt.axis('image')
    plt.title('Time: ' + str(time))
    plt.draw()

# Advance the simulation
grid = step(grid, new_grid)

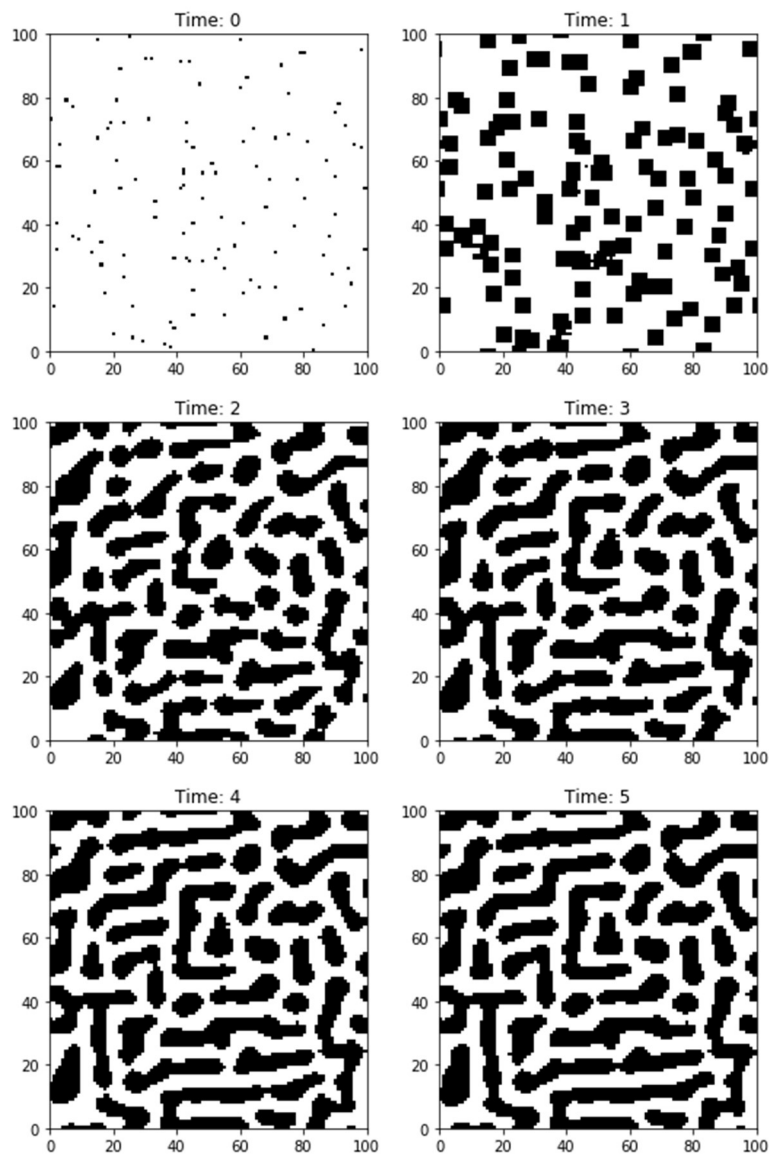
```

## APPENDIX B: EXTENDED CELLULAR AUTOMATON RESULTS

The figures provided here were generated by fixing the following simulation parameters:

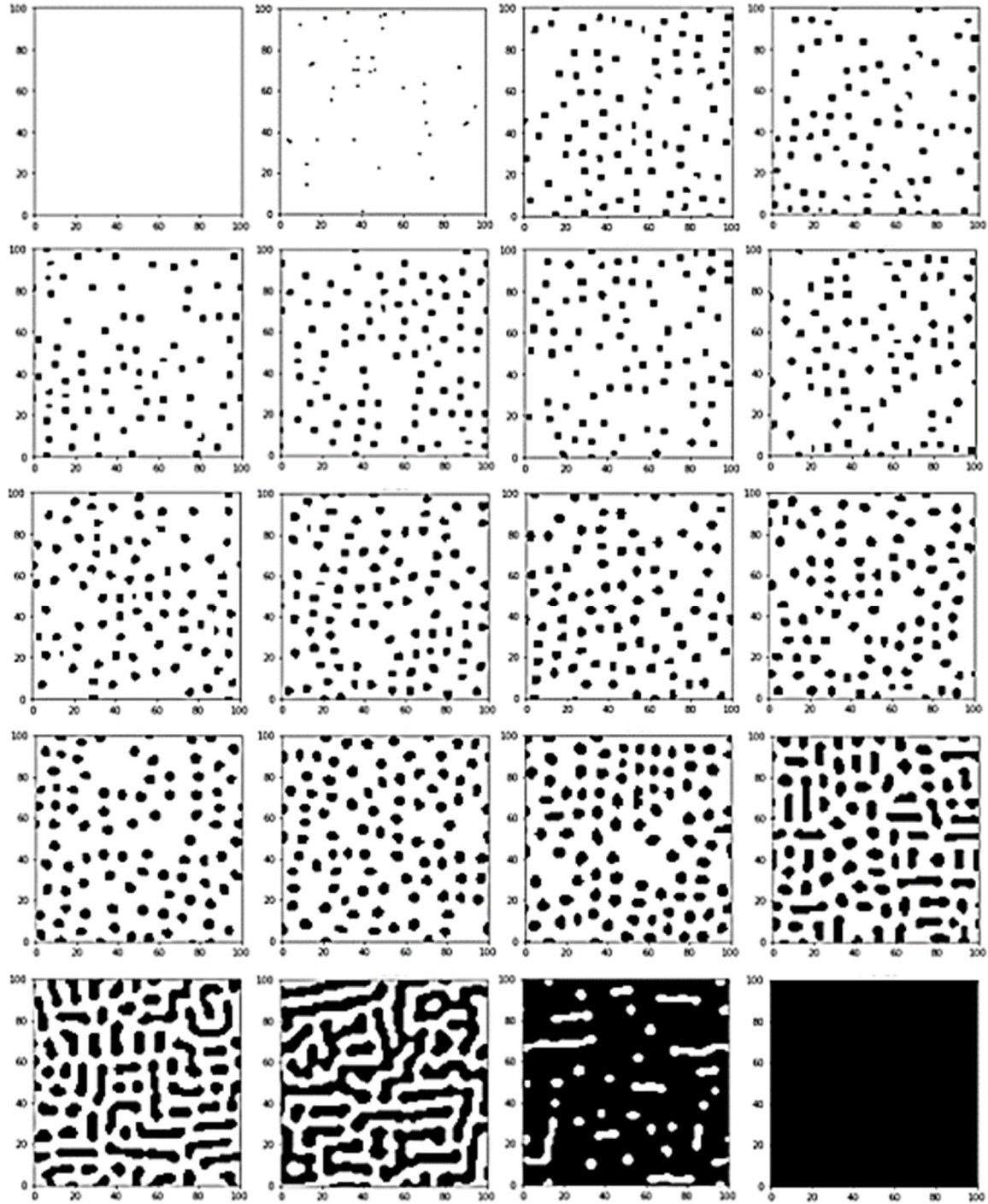
$$\begin{aligned}p &= 0.015 \\R_a &= 2 \\R_i &= 5 \\w_a &= 1\end{aligned}$$

### B1. EVOLUTION OVER TIME ( $w_2 = 0.2$ )



## B2. VARYING INHIBITOR FIELD VALUE (TIME-STEPS = 20)

The following plots were generated by varying the inhibitor field value  $w_2$  from 1.05 (upper left figure) to 0.10 (bottom right figure) in increments of 0.05:



## APPENDIX C: COMPUCELL3D CELLULAR POTTS MODEL CODE

### C1. MAIN PYTHON SCRIPT

```
from cc3d import CompuCellSetup

from cellsort_2DSteppables import cellsort_2DSteppable

CompuCellSetup.register_steppable(steppable=cellsort_2DSteppable(frequency=1))

CompuCellSetup.run()
```

### C2. XML SCRIPT

```
<CompuCell3D>
  <Potts>
    <Dimensions x="100" y="100" z="1"/>
    <Anneal>10</Anneal>
    <Steps>10000</Steps>
    <Temperature>10</Temperature>
    <Flip2DimRatio>1</Flip2DimRatio>
    <NeighborOrder>2</NeighborOrder>
  </Potts>

  <Plugin Name="Volume">
    <TargetVolume>25</TargetVolume>
    <LambdaVolume>2.0</LambdaVolume>
  </Plugin>

  <Plugin Name="CellType">
    <CellType TypeName="Medium" TypeId="0"/>
    <CellType TypeName="Condensing" TypeId="1"/>
    <CellType TypeName="NonCondensing" TypeId="2"/>
  </Plugin>

  <Plugin Name="Contact">
    <Energy Type1="Medium" Type2="Medium">0</Energy>
    <Energy Type1="NonCondensing" Type2="NonCondensing" >14</Energy>
    <Energy Type1="Condensing" Type2="Condensing" >14</Energy>
```

```

    <Energy Type1="NonCondensing" Type2="Condensing" >16</Energy>
    <Energy Type1="NonCondensing" Type2="Medium">16</Energy>
    <Energy Type1="Condensing" Type2="Medium">16</Energy>
    <NeighborOrder>2</NeighborOrder>
</Plugin>

<Steppable Type="BlobInitializer">

    <Region>
        <Center x="50" y="50" z="0"/>
        <Radius>40</Radius>
        <Gap>0</Gap>
        <Width>5</Width>
        <Types>Condensing,NonCondensing</Types>
    </Region>
</Steppable>

</CompuCell3D>

```

### C3. PYTHON SCRIPT

```

from cc3d.core.PySteppables import *

class cellsort_2DSteppable(SteppableBasePy):

    def __init__(self,frequency=1):

        SteppableBasePy.__init__(self,frequency)

    def start(self):
        """ any code in the start function runs before MCS=0 """

    def step(self,mcs):
        """ type here the code that will run every frequency MCS
        :param mcs: current Monte Carlo step """

    def finish(self):
        """ Finish Function is called after the last MCS """

```

## APPENDIX D: EXTENDED CELLULAR POTTS MODEL RESULTS

The following figures were generated after 3000 Monte Carlo Steps by fixing  $J_{M-M} = 0$  and  $J_{1-2} = J_{M-1} = J_{M-2} = 16$  and by varying the adhesion energy for cells of the same  $J_{p-p}$  ( $p = 1,2$ ) from 0.5 (upper left) to 18.0 (bottom right) in 0.5 increments of 0.5:

